High-Resolution Spectral Domain-OCT Imaging in Geographic Atrophy Associated with Age-Related Macular Degeneration

Monika Fleckenstein, Peter Charbel Issa, Hans-Martin Helb, Steffen Schmitz-Valckenberg, Robert P. Finger, Hendrik P. N. Scholl, Karin U. Loeffler, and Frank G. Holz

Purpose. To describe morphologic variations in outer retinal layers in eyes with atrophic age-related macular degeneration (AMD) using high-resolution, spectral-domain optical coherence tomography (SD-OCT).

Methods. SD-OCT scans were obtained with a combined confocal scanning laser ophthalmoscope (cSLO) and SD-OCT for simultaneous tomographic and topographic in vivo imaging. A total of 81 eyes of 56 patients (mean age, 77.8 ± 7.4 years) with geographic atrophy (GA) were examined. Morphologic alterations were analyzed and classified in the perilesional zone, at the junction between GA and nonatrophic retina, and in the atrophic area itself.

Results. In the perilesional zone, distinct morphologic alterations included elevations of the outer retinal layers, thickening, and spikes of the outer hyperreflective band as well as clumps at different neurosensory retinal levels. At the junction, highly variable transitions of the outer retinal layers were present with different degrees of loss of the normal hyperreflective bands. Within the actual GA, hyperreflective clumps at different retinal levels, segmented plaques of the outer band and elevations with variable reflectivity were visualized.

Conclusions. SD-OCT imaging in eyes with GA revealed a wide spectrum of morphologic alterations, both in the surrounding retinal tissue and in the atrophic area. These alterations may reflect different disease stages or, alternatively, heterogeneity on a cellular and molecular level. Longitudinal studies using in vivo SD-OCT imaging may allow evaluation of the relevance of these phenotypic changes as potential predictive markers for the progression of disease (i.e., enlargement rates of GA over time) and may be used for monitoring of future therapeutic interventions. (*Invest Ophthalmol Vis Sci.* 2008;49:4137–4144) DOI:10.1167/iovs.08-1967

From the Department of Ophthalmology, University of Bonn, Bonn, Germany.

Supported by the DFG (German Research Council), Research Priority Program Age-Related Macular Degeneration SPP 1088, Ho 1926/1-3; European Union FP6, Integrated Project Grant EVI-GENORET (LSHG-CT-2005-512036); and a DOG (German Society of Ophthalmology) research grant.

Submitted for publication March 3, 2008; revised April 9, 2008; accepted July 23, 2008.

Disclosure: **M. Fleckenstein**, Heidelberg Engineering (F); **P. Charbel Issa**, Heidelberg Engineering (F); **H.-M. Helb**, Heidelberg Engineering (F); **S. Schmitz-Valckenberg**, Heidelberg Engineering (F); **R.P. Finger**, Heidelberg Engineering (F); **H.P.N. Scholl**, Heidelberg Engineering (F); **K.U. Loeffler**, Heidelberg Engineering (F); **F.G. Holz**, Heidelberg Engineering (C, F)

The publication costs of this article were defrayed in part by page charge payment. This article must therefore be marked "*advertisement*" in accordance with 18 U.S.C. §1734 solely to indicate this fact.

Corresponding author: Frank G. Holz, Department of Ophthalmology, University of Bonn, Ernst-Abbe-Strasse 2, D-53127 Bonn, Germany; frank.holz@ukb.uni-bonn.de.

Age-related macular degeneration (AMD) is a complex disease with both genetic and environmental factors that has become the most common cause of legal blindness in industrialized countries.[1–8] It represents a chronic, progressive disease with various phenotypic manifestations, different disease stages, and variable rates of progression over time. Early manifestations of AMD include focal hypo- and hyperpigmentation and soft drusen with extracellular material accumulating in the inner aspects of Bruch's membrane. Geographic atrophy (GA) and choroidal neovascularization (CNV) represent the late stages of AMD. Although the incidence of neovascular AMD is higher overall than of GA, pure GA has recently been found to occur four times more often than neovascular AMD in individuals ≥85 years of age.[4] Natural history studies of GA, including the pivotal investigations by Sunness et al.[9–13] have identified various disease characteristics, including progression rates and functional consequences.[9–16] Current data reflect not only the public health impact of advanced atrophic AMD, but are also being used in the design of interventional trials.

Despite a recent breakthrough with anti-VEGF-therapy for neovascular AMD, there is as yet no treatment available for patients with GA. To identify potential targets for intervention, a better understanding of the pathogenesis of late atrophic AMD appears mandatory.

Recent developments in retinal imaging technologies have enabled more accurate phenotyping and provided further insights in the diseases process. Abnormal fundus autofluorescence patterns in atrophic AMD and their impact on disease progression has been intently studied with confocal scanning laser ophthalmoscopy (cSLO) imaging (Bindewald A, et al. *IOVS* 2004;45:ARVO E-Abstract 2960).[14–23] The findings implicate a role of excessive lipofuscin accumulation in the retinal pigment epithelium (RPE) and toxic fluorophores such as A2-E in the pathogenesis of outer retinal atrophy in the context of late AMD. With the advent of optical coherence tomography (OCT), vertical sections of the retina can be obtained in vivo with visualization of microstructural alterations in retinal diseases such as AMD. Recently, spectral-domain (SD) OCT technology has been introduced with further improvements in resolution and imaging speed compared with previous time-domain OCT imaging instruments.[24–32]

The combination of the two technologies (i.e., cSLO and SD-OCT) in one instrument, together with real-time eye tracking, now allows accurate orientation of vertical OCT scans at anatomic sites of interest with a pixel-to-pixel correlation and therefore provides three dimensional mapping of pathologic alterations within the retinal layers (Helb H-M, et al. *IOVS* 2007;48:ARVO E-Abstract 129). We used this imaging method to identify morphologic alterations in outer retinal layers in a systemic approach in eyes with GA due to AMD.

Methods

In a cross-sectional study, 81 eyes of 56 patients with late atrophic AMD (mean age, 77.8 ± 7.4) were examined by simultaneous cSLO

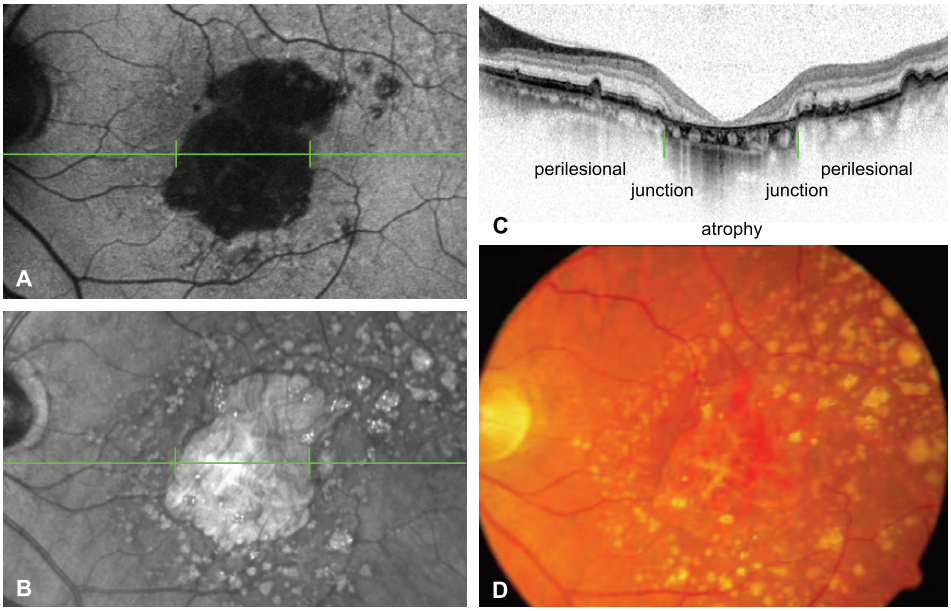

FIGURE 1. Fundus autofluorescence (**A**) and infrared reflectance (**B**) images with the corresponding SD-OCT scan (**C**) obtained by simultaneous cSLO and SD-OCT imaging in a 70-year-old patient with GA due to AMD. (**A**, **B**, *horizontal green lines*) Location of the SD-OCT scan (**C**). (**A–C**, *vertical green lines*) Junction between the atrophic patch and nonatrophic retina. (**D**) Corresponding fundus picture.

SD-OCT imaging. Patients (42 women and 14 men) with uni- or multifocal GA and overall clear media were enrolled. Exclusion criteria included the presence of signs of CNV or subretinal fibrosis and other retinal diseases in the study eye, such as diabetic retinopathy or hereditary retinal dystrophies, as well as any history of retinal surgery, laser photocoagulation, and radiation therapy. Before examination, the pupil of the study eye was dilated with 1% tropicamide eye drops.

Simultaneous recordings of SD-OCT and cSLO digital infrared or fundus autofluorescence (FAF) images were obtained with a novel combined imaging system (Spectralis HRA+OCT; Heidelberg Engineering, Heidelberg, Germany). The cSLO system provides fundus autofluorescence imaging (excitation wavelength: 488 nm, barrier filter; 500 nm), as well as infrared reflectance (IR; 820 nm) and blue (488 nm) reflectance imaging. The size of the field of view was 30° × 30°. Image acquisition was performed in high-speed mode. Images with 30° field of view are digitized in frames of 768 × 768 pixels with a resolution of approximately 11 μm per pixel. Optical resolution is approximately 10 μm. Image acquisition speed for a 30° field of view is nine images/s.

The SD-OCT runs simultaneously with the cSLO imaging system, using a second, independent pair of scanning mirrors. The wavelength of the SD-OCT imaging system is 870 nm. Optical resolution is approximately 7 μm in depth and 14 μm transversely. Acquisition speed is 40,000 A-scans per second. The scan depth is 1.8 mm. Each A-scan consists of 512 pixels, providing a digital depth resolution of 3.5 μm per pixels. Live B-scans can be acquired and observed simultaneously with a cSLO reference image that can be a confocal infrared or blue reflectance image, a fluorescein angiography image, or a fundus autofluorescence image. A B-scan covers a transverse range of 30° and consists of 768 A-scans in high-speed mode, which provides a digital transverse resolution of approximately 11 μm. B-scan acquisition speed for 30° scan width is 48 B-scans per second in high-speed mode. In high-speed mode, the vertical presentation of the OCT scan is magnified twice; therefore, morphologic alterations are presented disproportionately high in the vertical dimension.

The presence of atrophic areas was confirmed on cSLO FAF images with corresponding dark-appearing areas in the absence of the RPE cell monolayer and thus absence of fluorophores relevant for the FAF signal. Vertical and horizontal OCT scans were placed in the area of interest. Three different areas were analyzed with respect to alterations in the OCT scans: (1) the perilesional zone, which compasses retinal areas with visible abnormalities on fundus photograph, cSLO image, or OCT outside atrophic patches; (2) the junction between atrophic patches and nonatrophic retina, and (3) the atrophic patch itself (Fig. 1). Alterations within the SD-OCT scan were proportionally magnified for better visualization of alterations (Fig. 2).

The study adhered to the tenets of the Declaration of Helsinki. Informed consent was obtained from each patient after explanation of the nature and possible consequences of the study.

RESULTS

Normal Eye

The SD-OCT scan of the retina shows distinct bands that appear to correlate with the anatomic layers of the human retina (Fig. 3). However, there is still controversy as to the

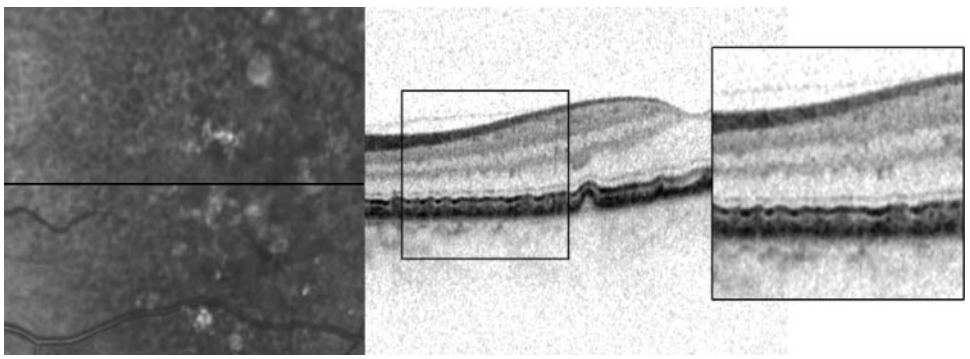

FIGURE 2. Combined infrared reflectance and SD-OCT image of an eye with a reticular drusen pattern. The area of interest is proportionally magnified for better visualization of the alterations in the SD-OCT scan.

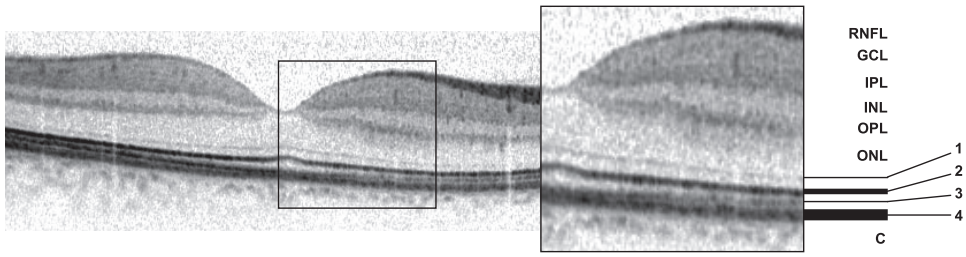

FIGURE 3. SD-OCT scan through the fovea of a normal retina of a 32-year-old man. Different hyperreflective bands can be defined that seem to correlate with the anatomic layers of the retina. However, there is still controversy in the labeling of the different bands. Among others, the following correspondence has been proposed by Pircher et al.[33] and was applied in this study to discuss morphologic alterations: (band 1) external limiting membrane (ELM), (band 2) interface of the inner and outer segments of the photoreceptor layer (IPRL), (band 3) outer segment-RPE interdigitation (OS/RPE), and (band 4) RPE/Bruch's membrane complex. These bands are referred to in Figures 4–7. RNFL, retinal nerve fiber layer; GCL, ganglion cell layer; IPL, inner plexiform layer; INL, inner nuclear layer; OPL, outer plexiform layer; ONL, outer nuclear layer; C, choriocapillaris and choroidea.

accurate labeling and histologic correlates of these bands, particularly of the distinct strongly reflective bands in the outer retina.[33,34] To discuss morphologic alterations in this study, the following correspondence has been applied.

A plausible morphologic substrate of the first hyperreflective band (Fig. 3, band 1) is the external limiting membrane (ELM). The second band (2) appears to reflect the interface of the inner and outer segments of the photoreceptor layer (IPRL), the third band (3) is assumed to represent the outer segment-RPE interdigitation (OS/RPE), and the fourth band (4) may reflect the RPE/Bruch's membrane complex.[33,35] It has been speculated that the separation of the third and the fourth hyperreflective bands, which is not always visible, is due to multiple scattering of large nonspherical particles (e.g., melanosomes) within the RPE.[33]

Perilesional Zone

Markedly heterogeneous changes were observed in the perilesional zone of GA, which encompassed retinal areas with visible abnormalities on the fundus photograph, SLO image, or OCT outside atrophic patches. In some sections, the retinal layers appeared without noticeable alterations either of the inner or the outer retinal layers (Fig. 4A). Band 3 was not always visible, particularly not in areas of altered bands 2 and 4. In some sections, the single bands 1 to 4 could not be defined at all (Figs. 4C, 4F, 4G).

Thinning and thickening of band 4 was a common finding (Fig. 4B). Highly reflecting, segmented plaques were noted in some sections at the level of band 4 (Fig. 4C, black arrow). These alterations correlated with highly reflective lesions in the IR image. Elongated elevations of band 4 were noted that did not correlate with funduscopically visible drusen (Fig. 4C); in contrast, many sections showed dome-shaped elevations of band 4 (Figs. 4D–F), correlating with drusen. Above, bands 1 and 2 were elevated (Fig. 4D), disrupted, or irregular in shape, so that the single band could no longer be differentiated (Figs. 4E, 4F). Beneath such elevations, a thin line at the former band 4 level was observed (Figs. 4C–F). The arising cavity in most sections appeared to be without backscattering material (Figs. 4D, 4E), whereas in some sections, irregularly hyperreflective material was present (Fig. 4F, black arrow).

Apical extensions of the thickened band 4 were observed, with and without associated disruptions in bands 1 and 2, respectively. Some had clumps at the tips in different retinal layers (Figs. 4G–I). Such vertical extensions had spikelike appearances, beginning at the level of band 4, with extension through the overlying bands (Fig. 4H).

At the level of the outer plexiform layer (OPL) clumps were noted that corresponded to patches of highly increased FAF in the cSLO image. The layers beneath such lesions were disrupted as if a piece of band 4 had been torn out and had broken through the layers above and was now localized at the assumed OPL level (Fig. 4J, black arrow).

Some sections showed small elevations of band 2 with a mottled irregular appearance of band 4 beneath (Fig. 4K). This alteration was commonly associated with a reticular drusen pattern in the FAF and IR images, respectively. Occasionally an increased distance between bands 2 and 4 were observed; however, this was an infrequent finding (Fig. 4L, black arrow).

In one eye of a patient, typically multiple such alterations were detected.

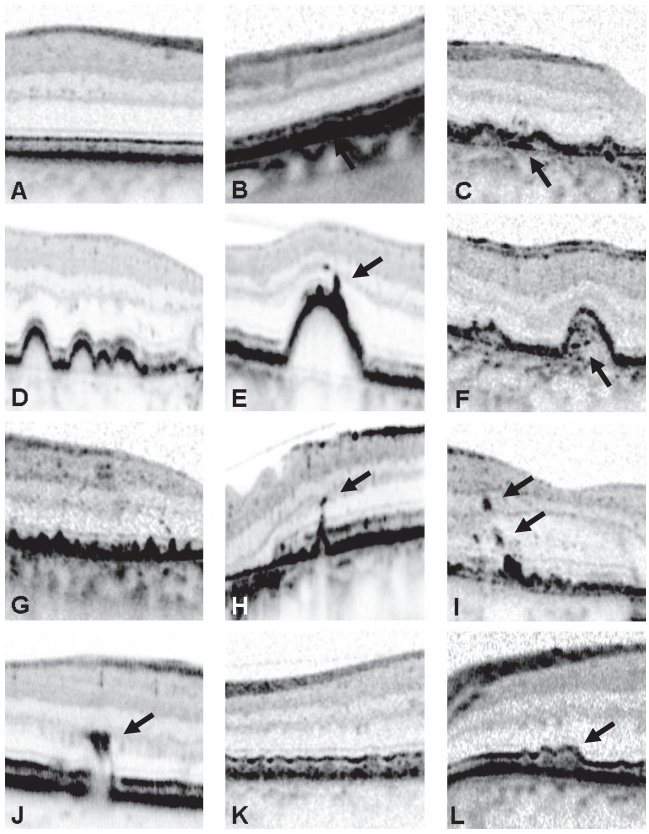

FIGURE 4. Heterogeneous alterations in the SD-OCT scans in the perilesional zone of atrophy. (**A**) Layers in clinically normal appearing retina; (**B**) thickening of band 4; (**C**) elongated elevation of band 4 with plaques beneath; (**D**) dome-shaped elevations with preserved layers above; (**E**) dome-shaped elevation with clumps at the top; (**F**) dome-shaped elevation with backscattering material beneath; (**G**) apical extensions of band 4; (**H**) spike with a clump at the tip; (**I**) clumps at different retinal levels; (**J**) clump in the OPL with disrupted bands beneath; (**K**) small elevations of band 2 and mottled band 4; and (**L**) increased distance between band 2 and band 4.

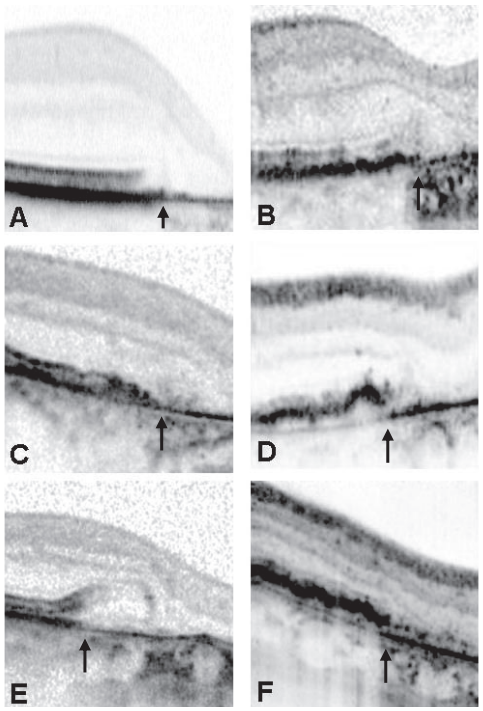

FIGURE 5. Heterogeneous shapes of the junction between the atrophic patch and nonatrophic retina visualized by SD-OCT. The edge was correlated pixel-for-pixel with the corresponding confocal scanning laser ophthalmoscopy image and is indicated with a *black arrow* (in all images, the atrophic patch is located on the right side). (**A**) Shifted endings of bands 2 and 4, with band 1 ending in a curved line; there was no irregular morphology of the bands just adjacent to the abrupt ending; a thin band remained as an extension of the lower part of band 4 within the atrophic patch; (**B**) irregular shape and ending of bands 1, 2, and 4; (**C**) at the edge, alterations obscured the delineations between the different outer retinal bands; (**D**) elevated band 4, decreased reflectivity of the band beneath, which remained after band 4 had thinned; (**E**) bands 1, 2, and 3 were elevated, while band 4 remained at its usual level before thinning; (**F**) elevated band 4 remained within the atrophy and had the appearance of a dotted line (Fig. 6B).

Junction between GA and Nonatrophic Retina

At the junction of the atrophic patches, various morphologic alterations were noted. These included abrupt breaks of bands 2 to 4 at identical points, as well as endings at different transverse extensions, and band 2 terminating earlier than band 4 (Fig. 5A). In most cases, a thin line extending the lower part of band 4 was noted that was also present throughout the atrophy (Figs. 5, 6, 7). Band 1 commonly ended in a curved line merging with the atrophy. The layer above, most likely representing the outer nuclear layer (ONL), was also commonly noted to disappear within the atrophic area. The backscattering layer anterior to this layer was also disrupted or appeared to rest directly on the thin remaining parts of band 4 (Figs. 5A, 6A).

In comparison to this regular edge (Fig. 5A), different irregular alterations of the bands were observed. Frequently, the changes obscured the delineation of the different bands (Figs. 5B, 5C).

Irregular thickening of band 4 was sometimes accompanied by irregular or disrupted bands 2 and 4, respectively (Figs. 5B, 5C). Band 4 was observed to end in an elevated position (Figs. 5D, 5F). In some sections, bands 1, 2, and 3 were raised with a thinned or normal thickened band 4 beneath (Fig. 5E).

In some eyes, the elevated band 4 remained in the form of a dotted line throughout the atrophy (Figs. 5F, 6B, 7E). When the OCT section cut through a small atrophic lesion, the termination of the bands and layers at the junction gave a funnel-shaped picture (Fig. 6A, black asterisk, right).

Atrophic Area

Corresponding to the area of atrophy, bands 1, 2, 3, and 4 as well as the assumed ONL were usually absent (Fig. 6A). The hyperreflective layer anteriorly also disappeared or appeared to be present adjacent to the thin band that remained as an extension of the lower part of band 4 (Fig. 6A). Plaques at the former level of band 4 were observed (Fig. 6B) that correlated with highly reflective lesions in the IR image.

In most sections, clumps that rested on the thin remainder of band 4 where scattered throughout the atrophy (Fig. 7C). In some sections, clumps in different retinal layers were noted (Fig. 7D). Within some patches, the elevated band 4 seemed to

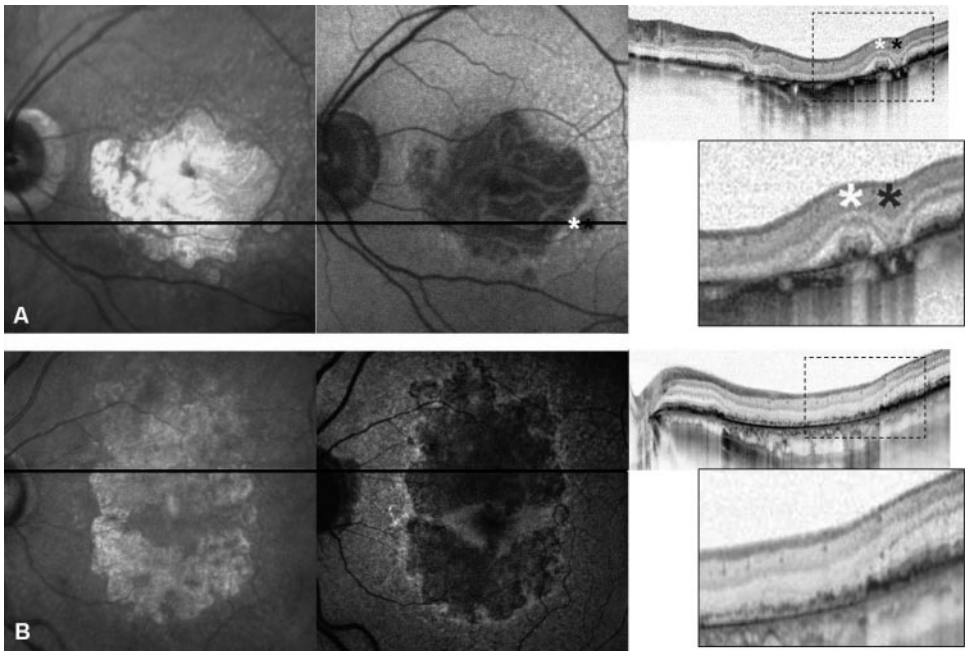

FIGURE 6. Combined SD-OCT and confocal scanning laser ophthalmoscopy IR and FAF imaging through the entire atrophic area. (**A**) When the OCT section cut through a small atrophic lesion, the terminating bands and layers at the junction had a funnel-shaped appearance (*black asterisk*). The emerging layers on both sides of an islands or bridge of preserved retina had a dome-shaped appearance (*white asterisk*). Within the atrophic spot, bands 1, 2, 3, and 4 as well as the assumed ONL were usually absent. (**B**) In contrast to (**A**), band 4 remained, appearing as an elevated, thin dotted line within the atrophy; beneath, there was a continuous band of increased reflectivity.

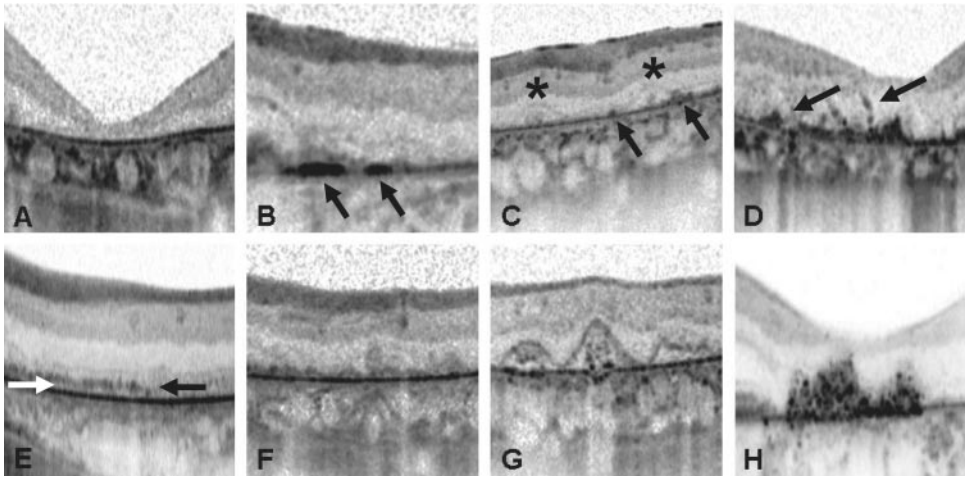

FIGURE 7. Alterations within the atrophic area visualized by SD-OCT. (**A**) Loss of the outer retinal layers and remaining line in extension of the lower part of band 4; (**B**) plaques at the former band 4 level (*arrows*); (**C**) elevations (*asterisks*) and clumps (*arrows*) at the remaining line in extension of the lower part of band 4; (**D**) clumps (*arrows*) at different retinal levels; (**E**) dotted-line–appearing formation that remained as an extension of the elevated band 4 (*black arrow*; see Figs. 5F, 6B); beneath, there was a continuous hyperreflective band (*white arrow*); (**F**) irregular elevations at the remaining extension of the lower part of band 4; (**G**) crownlike elevations with "debris" beneath; (**H**) accumulation of irregular, highly reflective material.

remain as a thin dotted line throughout the atrophy (Figs. 5F, 6B, 7E); beneath, there was a continuous hyperreflective band.

There were also sections showing elevations at the remainder of band 4 (Fig. 7F). In some sections, there where elevations with crownlike appearance with presumed debris beneath these structures (Fig. 7G). These lesions correlated with an increased FAF signal within the atrophy. In the IR image, small hyperreflective dots were typically located adjacent to those lesions. Distinguishable from those alterations, there were accumulations with irregularly reflecting material in the OCT scan that correlated with highly reflecting lesions in the IR images (Fig. 7H).

Typically, the presumptive OPL or inner nuclear layer (INL) rested on the lesions noted within the atrophy. In contrast to those lesions, there were islands within the atrophic patch with preserved bands 1, 2, and 4 and the presumptive ONL and OPL. In those areas the layers often showed alterations but were distinguishable from each other. The emerging layers on both sides of these islands gave a dome-shaped appearance (Fig. 6A, white asterisk, right).

In one eye of a patient, different alterations within the atrophic area may occur.

DISCUSSION

Examination by high-resolution OCT allows for visualization of microstructural alterations of the inner and outer retinal layers in vivo. With the advent of high-resolution OCT imaging new insights in phenotypic variations in the disease can now be obtained. While the clinical presentation of GA associated with AMD on funduscopy or two-dimensional images such as fundus photography appears relatively uniform, a wide, complex spectrum of heterogeneous alterations can be identified in SD-OCT scans.

Previous reports not specifically focusing on atrophic AMD have recently addressed some findings on SD-OCT images.[25,35–39] The goal of the present study was to identify and demonstrate the broad spectrum of morphologic alterations that can be visualized by high-resolution OCT imaging and to allocate these changes to the different zones in eyes with late atrophic AMD.

By applying the morphologic substrates proposed by Pircher et al.,[33] alterations of the different bands in the OCT scans can be correlated with findings reported in histologic studies in eyes with AMD (Fig. 8).[40–44] In the perilesional zone of primary GA, RPE cells are irregular in shape, some being enlarged and others attenuated; closer to the junction, the RPE becomes increasingly disorganized. Cells that are packed with pigment granules are shed into more inner retinal layers. Photoreceptor outer segments may terminate in rounded collections of membranes lying on the internal surface of the RPE, each partly surrounded by broad apical extensions from the RPE cells. Sub-RPE deposits and hyalinization and densification of Bruch's membrane can be observed. The closer to the junction of GA, the more grossly abnormal the photoreceptors become.

Although ultrastructural changes cannot be visualized by OCT imaging so far, alterations of the outer retinal layers including the RPE layer can be observed that may be in accordance with histopathologic findings. Thinning or thickening of the RPE band (band 4) in the OCT scan may indeed reflect boundaries of enlarged or attenuated RPE cells. Hyperreflective clumps at different retinal layers can be visualized that correlate with funduscopically visible hyperpigmentary changes; these findings are in accordance with recently reported RPE changes imaged by ultrahigh resolution OCT in eyes with nonexudative AMD by Pieroni et al.[38]

Besides soft drusen that present as dome-shaped elevations of the RPE band in OCT, more elongated elevations can be observed that may be consistent with sub-RPE deposits (e.g., basement membrane deposits)[45]; however, the localization with respect to the basement membrane of the RPE cannot be clearly determined by OCT. Variations in reflectivity of such sub-RPE deposits detected in our study may reflect different compositions of the underlying material. The thin line that was seen in some sections at the former RPE level in the area of such elevations may indeed represent Bruch's membrane[35]; hyperreflective plaques at this level may represent histologically described densification.[41,42] Attenuation or disappear-

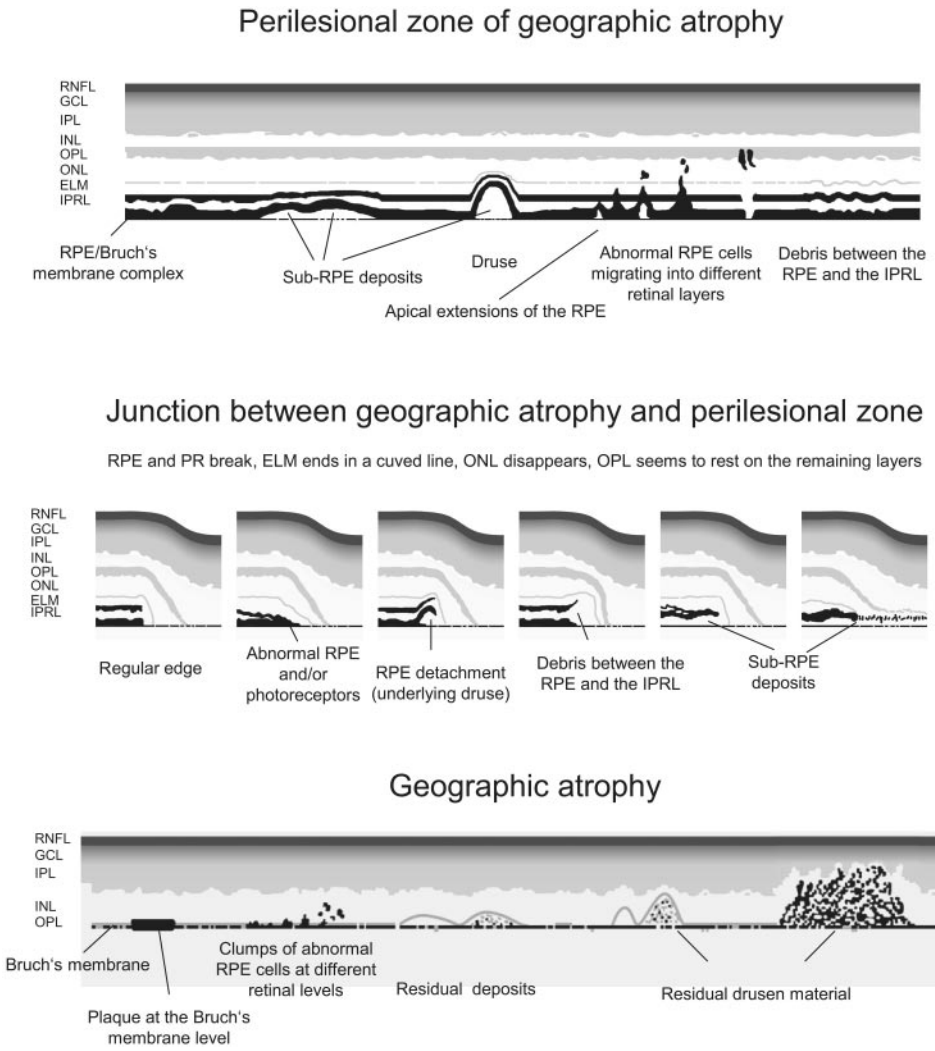

FIGURE 8. Interpretation of alterations on SD-OCT scans in eyes with late atrophic AMD. SD-OCT findings in the perilesional zone, at the junction between GA and nonatrophic retina and within the atrophic patch are shown, and possible morphologic correlates are illustrated. Different combinations of these alterations can be found in one eye of the same patient. Changes in the perilesional zone may not be specifically related to GA but rather represent changes occurring in early dry AMD. RNFL, retinal nerve fiber layer; GCL, ganglion cell layer; IPL, inner plexiform layer; INL, inner nuclear layer; OPL, outer plexiform layer; ONL, outer nuclear layer; ELM, external limiting membrane; IPRL, interface of the inner and outer segments of the photoreceptor layer; RPE, retinal pigment epithelium.

ance of the IPRL in the OCT scans seems to be in accordance with morphologic alterations of the photoreceptors in the perilesional zone.

Above soft drusen, alterations of the RPE, IPRL (band 2), ELM (band 1) and ONL, respectively, can be observed by OCT imaging; this observation is in accordance with the histologic findings in drusen-related atrophy, where the degeneration of the RPE preferentially occurs over drusen and photoreceptors and the ONL subsequently disappear.

In areas with a reticular drusen pattern in the cSLO image, small elevations of the IPRL band were noted along with a mottled irregular appearance of the RPE band; however, the exact origin of the reticular signal could not be determined. Thus, the exact location of reticular drusen, at this stage, remains unclear.

Increased distance between the IPRL and RPE band with the impression of accumulating material between the RPE and the photoreceptors could be consistent with debris lying in the subretinal space which has been described in histologic sections in eyes with GA. It has been discussed that this debris may represent outer segment material that has not been phagocytosed.[42]

Funduscopically visible abnormalities surrounding atrophy in GA resemble typical changes seen in early dry AMD, such as various types of drusen or hyper- or hypopigmentations. It is conceivable that the structural alterations revealed by SD-OCT at the perilesional zone of the patients with GA in this study may also represent general AMD changes and may therefore not be specific for GA.

At the junction of GA, histologic sections have revealed that the termination of the RPE may be characterized by a double layer of cells. The overlying photoreceptors may disappear for some distance beyond the edge or together with the RPE, and the ELM ends in a curved line; the ONL disappears and an attenuated OPL rests directly on Bruch's membrane or the remaining sub-RPE deposits; the INL is reported to be less affected.[42] In the OCT sections, similar alterations are visualized. However, different variations of this "regular" edge are observed that may reflect different patterns of development and/or progression of GA (e.g., primary atrophy, drusen-related atrophy, or atrophy after RPE detachments as described by Sarks and Sarks).[40]

Within the atrophic area, occasional whorls of persisting photoreceptors converging on a cluster of degenerating pigment cells have been reported by histopathology. Elsewhere, the photoreceptors disappear, but a few grossly abnormal RPE cells or membrane-bound bodies containing pigment commonly remain scattered throughout the area.[42] Accordingly, by OCT imaging, islands with preserved layers (i.e., RPE-, IPRL-band, ELM, ONL, and OPL) are noted that correlate with a preserved FAF signal in the cSLO image. Within other sections, hyperreflective clumps at different retinal levels can be visualized, but the outer retinal layers are not present.

Elevations or accumulations of highly reflective material within the atrophic area as well as plaques at the former RPE level can be observed by OCT imaging. These alterations may represent residual sub-RPE deposits and may reflect various stages of regressing drusen, which become calcified and increasingly irregular.[41,42] It has been postulated that regressing drusen material may remain in the atrophic area for many years. Its presence may refer to drusen-related evolution of the atrophic lesion.

Various limitations of this study must be considered. First, alterations of reflectivity are yet not readily correlated with physiological anatomic layers in normal eyes. Interpretation becomes even more difficult in the presence of complex pathologic alterations.[34] Therefore, misinterpretations of hyperreflective bands, especially in outer retinal layers, become an obstacle. Second, various morphologic alterations may be present in different vertical scans of the same eye. However, the goal of this study was to describe for the first time the spectrum of morphologic variations seen on SD-OCT in the different zones in eyes with GA, in an attempt to classify these alterations. By scrutinizing all vertical layers, future studies will address, to what extent the described alterations may be specific to individual eyes. Longitudinal observations over a longer period will help in understanding the evolution of the changes seen in this cross-sectional review. Furthermore, it would be helpful in future studies to correlate SD-OCT findings in images obtained in vivo with the histopathologic findings postmortem in donor eyes with atrophic AMD.

SD-OCT imaging in eyes with late atrophic AMD revealed highly variable morphologic alterations in the atrophic area and in the surrounding retinal tissue. These alterations may reflect both different stages of the disease and heterogeneity on a cellular and molecular level. Longitudinal studies using in vivo SD-OCT imaging will allow evaluation of the relevance of distinct phenotypic changes as potential predictive markers for the progression of disease (i.e., enlargement rates of atrophic areas).

References

1. Ambati J, Ambati BK, Yoo SH, Ianchulev S, Adamis AP. Age-related macular degeneration: etiology, pathogenesis, and therapeutic strategies. *Surv Ophthalmol*. 2003;48:257–293.
2. Chakravarthy U, Augood C, Bentham GC, et al. Cigarette smoking and age-related macular degeneration in the EUREYE Study. *Ophthalmology*. 2007;114:1157–1163.
3. Klaver CC, Wolfs RC, Vingerling JR, Hofman A, de Jong PT. Age-specific prevalence and causes of blindness and visual impairment in an older population: The Rotterdam Study. *Arch Ophthalmol*. 1998;116:653–658.
4. Klein R, Klein BE, Knudtson MD, Meuer SM, Swift M, Gangnon RE. Fifteen-year cumulative incidence of age-related macular degeneration: The Beaver Dam Eye Study. *Ophthalmology*. 2007; 114:253–262.
5. Tomany SC, Wang JJ, Van LR, et al. Risk factors for incident age-related macular degeneration: pooled findings from 3 continents. *Ophthalmology*. 2004;111:1280–1287.
6. van Leeuwen R, Klaver CC, Vingerling JR, Hofman A, de Jong PT. Epidemiology of age-related maculopathy: a review. *Eur J Epidemiol*. 2003;18:845–854.
7. Wang JJ, Rochtchina E, Lee AJ, et al. Ten-year incidence and progression of age-related maculopathy: the blue Mountains Eye Study. *Ophthalmology*. 2007;114:92–98.
8. Augood CA, Vingerling JR, de Jong PT, et al. Prevalence of age-related maculopathy in older Europeans: the European Eye Study (EUREYE). *Arch Ophthalmol*. 2006;124:529–535.
9. Sunness JS, Rubin GS, Applegate CA, et al. Visual function abnormalities and prognosis in eyes with age-related geographic atrophy of the macula and good visual acuity. *Ophthalmology*. 1997;104: 1677–1691.
10. Sunness JS. The natural history of geographic atrophy, the advanced atrophic form of age-related macular degeneration. *Mol Vis*. 1999;5:25.
11. Sunness JS, Gonzalez-Baron J, Applegate CA, et al. Enlargement of atrophy and visual acuity loss in the geographic atrophy form of age-related macular degeneration. *Ophthalmology*. 1999;106: 1768–1779.
12. Sunness JS, Applegate CA, Bressler NM, Hawkins BS. Designing clinical trials for age-related geographic atrophy of the macula: enrollment data from the geographic atrophy natural history study. *Retina*. 2007;27:204–210.
13. Sunness JS, Margalit E, Srikumaran D, et al. The long-term natural history of geographic atrophy from age-related macular degeneration: enlargement of atrophy and implications for interventional clinical trials *Ophthalmology*. 2007;114:271–277.
14. Holz FG, Bindewald-Wittich A, Fleckenstein M, Dreyhaupt J, Scholl HPN, Schmitz-Valckenberg S. Progression of geographic atrophy and impact of fundus autofluorescence patterns in age-related macular degeneration. *Am J Ophthalmol*. 2007;143:463–472.
15. Schmitz-Valckenberg S, Bultmann S, Dreyhaupt J, Bindewald A, Holz FG, Rohrschneider K. Fundus autofluorescence and fundus perimetry in the junctional zone of geographic atrophy in patients with age-related macular degeneration. *Invest Ophthalmol Vis Sci*. 2004;45:4470–4476.
16. Schmitz-Valckenberg S, Bindewald-Wittich A, Dolar-Szczasny J, et al. Correlation between the area of increased autofluorescence surrounding geographic atrophy and disease progression in patients with AMD. *Invest Ophthalmol Vis Sci*. 2006;47:2648–2654.
17. Bindewald A, Schmitz-Valckenberg S, Jorzik JJ, et al. Classification of abnormal fundus autofluorescence patterns in the junctional zone of geographic atrophy in patients with age related macular degeneration. *Br J Ophthalmol*. 2005;89:874–878.
18. Holz FG, Bellmann C, Staudt S, Schütt F, Völcker HE. Fundus autofluorescence and development of geographic atrophy in age-related macular degeneration. *Invest Ophthalmol Vis Sci*. 2001; 42:1051–1056.
19. Holz FG, Bellmann C, Margaritidis M, Schutt F, Otto TP, Volcker HE. Patterns of increased in vivo fundus autofluorescence in the junctional zone of geographic atrophy of the retinal pigment epithelium associated with age-related macular degeneration. *Graefes Arch Clin Exp Ophthalmol*. 1999;237:145–152.
20. Holz FG, Pauleikhoff D, Klein R, Bird AC. Pathogenesis of lesions in late age-related macular disease. *Am J Ophthalmol*. 2004;137: 504–510.
21. Bellmann C, Holz FG, Schapp O, Volcker HE, Otto TP. Topographie der Fundusautofluoreszenz mit einem neuen konfokalen Scanning-Laser-Ophthalmoskop. *Ophthalmologe*. 1997;94:385–391.
22. Lois N, Owens SL, Coco R, Hopkins J, Fitzke FW, Bird AC. Fundus autofluorescence in patients with age-related macular degeneration and high risk of visual loss. *Am J Ophthalmol*. 2002;133:341–349.
23. Smith RT, Chan JK, Busuoic M, Sivagnanavel V, Bird AC, Chong NV. Autofluorescence characteristics of early, atrophic, and high-risk fellow eyes in age-related macular degeneration. *Invest Ophthalmol Vis Sci*. 2006;47:5495–5504.
24. Drexler W, Morgner U, Ghanta RK, Kartner FX, Schuman JS, Fujimoto JG. Ultrahigh-resolution ophthalmic optical coherence tomography. *Nat Med*. 2001;7:502–507.
25. Drexler W, Sattmann H, Hermann B, et al. Enhanced visualization of macular pathology with the use of ultrahigh-resolution optical coherence tomography. *Arch Ophthalmol*. 2003;121:695–706.
26. Drexler W, Morgner U, Kartner FX, et al. In vivo ultrahigh-resolution optical coherence tomography. *Opt Lett*. 1999;24:1221–1223.
27. Drexler W. Ultrahigh-resolution optical coherence tomography. *J Biomed Opt*. 2004;9:47–74.
28. Cense B, Chen TC, Nassif N, et al. Ultra-high speed and ultra-high resolution spectral-domain optical coherence tomography and optical Doppler tomography in ophthalmology. *Bull Soc Belge Ophtalmol*. 2006:123–132.
29. Wojtkowski M, Bajraszewski T, Gorczynska I, et al. Ophthalmic imaging by spectral optical coherence tomography. *Am J Ophthalmol*. 2004;138:412–419.

30. Wojtkowski M, Bajraszewski T, Targowski P, Kowalczyk A. Real-time in vivo imaging by high-speed spectral optical coherence tomography. *Opt Lett*. 2003;28:1745–1747.
31. Nassif N, Cense B, Park BH, et al. In vivo human retinal imaging by ultrahigh-speed spectral domain optical coherence tomography. *Opt Lett*. 2004;29:480–482.
32. de Boer JF, Cense B, Park BH, Pierce MC, Tearney GJ, Bouma BE. Improved signal-to-noise ratio in spectral-domain compared with time-domain optical coherence tomography. *Opt Lett*. 2003;28:2067–2069.
33. Pircher M, Gotzinger E, Findl O, et al. Human macula investigated in vivo with polarization-sensitive optical coherence tomography. *Invest Ophthalmol Vis Sci*. 2006;47:5487–5494.
34. Drexler W. Cellular and functional optical coherence tomography of the human retina: the Cogan lecture 1. *Invest Ophthalmol Vis Sci*. 2007;48:5339–5351.
35. Michels S, Pircher M, Geitzenauer W, et al. Value of polarisation-sensitive optical coherence tomography in diseases affecting the retinal pigment epithelium 13. *Br J Ophthalmol*. 2008;92:204–209.
36. Ahlers C, Michels S, Elsner H, Birngruber R, Pruente C, Schmidt-Erfurth U. Topographic angiography and optical coherence tomography: a correlation of imaging characteristics. *Eur J Ophthalmol*. 2005;15:774–781.
37. Schmidt-Erfurth U, Leitgeb RA, Michels S, et al. Three-dimensional ultrahigh-resolution optical coherence tomography of macular diseases. *Invest Ophthalmol Vis Sci*. 2005;46:3393–3402.
38. Pieroni CG, Witkin AJ, Ko TH, et al. Ultrahigh resolution optical coherence tomography in non-exudative age related macular degeneration. *Br J Ophthalmol*. 2006;90:191–197.
39. Ko TH, Fujimoto JG, Schuman JS, et al. Comparison of ultrahigh- and standard-resolution optical coherence tomography for imaging macular pathology. *Ophthalmology*. 2005;112:1922–1935.
40. Sarks SH, Sarks JP. Age-related macular degeneration: atrophic form. In: Ryan SJ, Schachat AP, Murphy RM, eds. *Retina.* St. Louis: Mosby; 1994:1071–1102.
41. Green WR, Key SN, III. Senile macular degeneration: a histopathologic study. *Trans Am Ophthalmol Soc*. 1977;75:180–254.
42. Sarks JP, Sarks SH, Killingsworth MC. Evolution of geographic atrophy of the retinal pigment epithelium. *Eye*. 1988;2:552–577.
43. Messmer EP, Ruggli GH, Apple DJ, Naumann GOH. Spezielle Pathologie der Retina. In: Naumann GOH, ed. *Pathologie des Auges.* Berlin: Springer-Verlag; 1997:1089–1099.
44. Bressler SB, Bressler NM, Sarks SH, Sarks JP. Age-related macular degeneration: nonneovascular early AMD, intermediate AMD, and geographic atrophy. In: Ryan SJ, ed. *Retina*. 4th ed. Philadelphia: Elsevier Inc.; 2006:1041–1074.
45. Loeffler KU, Lee WR. Terminology of sub-RPE deposits: do we all speak the same language? *Br J Ophthalmol*. 1998;82:1104–1105.